

Superconductivity in $CuIr_{2-x}Al_xTe_4$ telluride chalcogenides

Dong Yan(严冬), Lingyong Zeng(曾令勇), Yijie Zeng(曾宜杰), Yishi Lin(林一石), Junjie Yin(殷俊杰),Meng Wang(王猛), Yihua Wang(王熠华), Daoxin Yao(姚道新), and Huixia Luo(罗惠霞)

Citation: Chin. Phys. B, 2022, 31 (**3**): 037406. DOI: 10.1088/1674-1056/ac43b1

Journal homepage: http://cpb.iphy.ac.cn; http://iopscience.iop.org/cpb

What follows is a list of articles you may be interested in

Electronic properties and interfacial coupling in Pb islands on single-crystalline graphene

Jing-Peng Song(宋靖鹏) and Ang Li(李昂)

Chin. Phys. B, 2022, 31 (**3**): 037401. DOI: 10.1088/1674-1056/ac1b8e

Evolution of superconductivity and charge order in pressurized RbV_3Sb_5

Feng Du(杜锋), Shuaishuai Luo(罗帅帅), Rui Li(李蕊), Brenden R. Ortiz, Ye Chen(陈晔), Stephen D. Wilson, Yu Song(宋宇), and Huiqiu Yuan(袁辉球)

Chin. Phys. B, 2022, 31 (**1**): 017404. DOI: 10.1088/1674-1056/ac4232

Revealing the A_{1g}-type strain effect on superconductivity and nematicity in FeSe thin flake

Zhaohui Cheng(程朝晖), Bin Lei(雷彬), Xigang Luo(罗习刚), Jianjun Ying(应剑俊), Zhenyu Wang(王震宇), Tao Wu(吴涛), and Xianhui Chen(陈仙辉)

Chin. Phys. B, 2021, 30 (**9**): 097403. DOI: 10.1088/1674-1056/ac1efa

Barrier or easy-flow channel: The role of grain boundary acting on vortex motion in type-II superconductors

Yu Liu(刘宇), Xiao-Fan Gou(苟晓凡), and Feng Xue(薛峰)

Chin. Phys. B, 2021, 30 (**9**): 097402. DOI: 10.1088/1674-1056/ac11ea

Excess-iron driven spin glass phase in $Fe_{1+y}Te_{1-x}Se_x$

Long Tian(田龙), Panpan Liu(刘盼盼), Tao Hong(洪涛), Tilo Seydel, Xingye Lu(鲁兴业), Huiqian Luo(罗会仟), Shiliang Li(李世亮), and Pengcheng Dai(戴鹏程)

Chin. Phys. B, 2021, 30 (**8**): 087402. DOI: 10.1088/1674-1056/ac0695

Superconductivity in $CuIr_{2-x}Al_xTe_4$ telluride chalcogenides

Dong Yan(严冬)[1,5,†], Lingyong Zeng(曾令勇)[1,†], Yijie Zeng(曾宜杰)[2,6], Yishi Lin(林一石)[3,4], Junjie Yin(殷俊杰)[2], Meng Wang(王猛)[2], Yihua Wang(王熠华)[3,4], Daoxin Yao(姚道新)[2], and Huixia Luo(罗惠霞)[1,‡]

[1] *School of Materials Science and Engineering, State Key Laboratory of Optoelectronic Materials and Technologies, Key aboratory of Polymer Composite & Functional Materials, Guangzhou Key Laboratory of Flexible Electronic Materials and Wearable Devices, Sun Yat-Sen University, Guangzhou* 510275, *China*

[2] *Center for Neuron Science and Technology, School of Physics, Sun Yat-Sen University, Guangzhou* 510275, *China*

[3] *State Key Laboratory of Surface Physics and Department of Physics, Fudan University, Shanghai* 200433, *China*

[4] *Shanghai Research Center for Quantum Sciences, Shanghai* 201315, *China*

[5] *Key Laboratory of Functional Molecular Solids, Ministry of Education, College of Chemistry and Materials Science, Anhui Normal University, Wuhu* 241002, *China*

[6] *College of Science, Hangzhou Dianzi University, Hangzhou* 310018, *China*

(Received 16 November 2021; revised manuscript received 10 December 2021; accepted manuscript online 16 December 2021)

The relationship between charge-density-wave (CDW) and superconductivity (SC), two vital physical phases in condensed matter physics, has always been the focus of scientists' research over the past decades. Motivated by this research hotspot, we systematically studied the physical properties of the layered telluride chalcogenide superconductors $CuIr_{2-x}Al_xTe_4$ ($0 \leqslant x \leqslant 0.2$). Through the resistance and magnetization measurements, we found that the CDW order was destroyed by a small amount of Al doping. Meanwhile, the superconducting transition temperature (T_c) kept changing with the change of doping amount and rose towards the maximum value of 2.75 K when $x = 0.075$. The value of normalized specific heat jump ($\Delta C/\gamma T_c$) for the highest T_c sample $CuIr_{1.925}Al_{0.075}Te_4$ was 1.53, which was larger than the BCS value of 1.43 and showed the bulk superconducting nature. In order to clearly show the relationship between SC and CDW states, we propose a phase diagram of T_c vs. doping content.

Keywords: layered telluride chalcogenide, superconductivity, charge-density-wave, $CuIr_{2-x}Al_xTe_4$

PACS: 74.70.Xa, 74.25.−q, 74.25.Dw, 71.45.Lr **DOI:** 10.1088/1674-1056/ac43b1

1. Introduction

The continuous suppression of metal–insulator (MI) transition, charge-density-wave (CDW) transition, magnetism, etc. leading to the occurrence of superconductivity (SC) in the proximity of such quantum states has garnered great interest and widespread study in solid-state physics.[1–4] The phase diagrams of unconventional high-temperature (high-T_c) cuprates and iron-based superconductors exemplified such phenomena.[5–11] Nevertheless, how SC emerges in these high-T_c superconductors is intricate and remains extremely puzzling. It is still essential to sort out the interplay between the SC and the other quantum states, promoting further understanding of the mechanism of high-T_c superconductors.

Low-dimensional layered transition metal dichalcogenides (TMDs) are other opportune material platforms for the exploration of various quantum instabilities,[12–21] especially the interplay between SC and CDW, in which the CDW order refers to condensate with periodic modulations of the crystalline lattice and conduction electron density in real space. Typically, the SC can be induced and a dome-shape superconducting phase diagram is formed upon suppressing the CDW order,[22–27] which is highly similar to the phase diagrams of unconventional high-T_c cuprates and iron-based superconductors. Despite overall phase diagram similarities, there are significant differences especially between their mechanisms, where unconventional high-T_c Fe-based and cuprate superconductors cannot be well explained by Bardeen–Cooper–Schrieffer (BCS) theory but most of the TMD superconductors can be explained by BCS theory. It has been generally considered that the collapse of CDW state accompanied by the improvement of superconducting transition temperature (T_c) is in reference to the abrupt enhancement of density of states (DOS) around the Fermi level $N(E_F)$ in the conventional superconductors owning to CDW state gaps out some regions of the Fermi surface.[1,2] The formation of Cu_xTiSe_2 ($0 \leqslant x \leqslant 0.1$) from intercalating the Cu into 1T-$TiSe_2$ exemplified a vivid phase diagram in the TMDs family,[2] and further evoked the continuous interest in searching for new superconductors in TMD materials by gating, adding physical pressures, chemical doping or point contact method.[22–38] For example, Cu-intercalation 2H-TaS_2 forms Cu_xTaS_2 ($0 \leqslant x \leqslant 0.12$) and displays an enhancement of T_c from 0.8 K ($x = 0$) to 4.5 K ($x = 0.04$).[34] In addition, experiments show that the T_c of WTe_2 can be increased to 7 K under an applied physical pressure of 16.8 GPa.[35] Moreover, manifold phase transitions from MI to metal show in 1T-TaS_2 thin flakes with collapses of CDWs, and finally SC are induced by ionic gating.[36]

[†]These authors contributed equally.

[‡]Corresponding author. E-mail: luohx7@mail.sysu.edu.cn

© 2022 Chinese Physical Society and IOP Publishing Ltd

Currently, $CuIr_2Te_4$, adopting a NiAs defected structure of trigonal symmetry with the space group P-3m1, has been found to exhibit the coexistence of the CDW-like transition ($T_{CDW} = 250$ K on heating and 186 K on cooling) and SC ($T_c = 2.5$ K). Besides, recent electronic structure calculations have unveiled that the Fermi energy is mostly derived from Ir 5d and Te 5p orbitals.[39] More recently, experiments have documented that both CDW and SC performances of $CuIr_2Te_4$ can be modified via 3d, 4d transition metals (e.g., Ti and Ru) and 4p, 5p dopants (e.g., Se and I). Dome-shape phase diagrams with respect to T_c vs. doping amount associated with the suppression of CDW have been found in the $CuIr_{2-x}Ru_xTe_4$ and $CuIr_{2-x}Ti_xTe_4$ systems, but dome-shape diagrams crowded in the middle doping region with two CDW regions at two sides in Se- and I-doped systems.[40–43] Furthermore, the non-magnetic element Al is usually selected as the dopant because Al^{3+} ion has a closed shell electron configuration and a clear oxidation state. The transport properties of Al-doped high-T_c copper-based superconductors (e.g., $SmBa_2Cu_{3-x}Al_xO_{6+\delta}$, $YBa_2Cu_{3-x}Al_xO_7$) have been widely studied.[44,45] And nano Al has been used to improve the critical current in MgB_2 superconductor.[46] Therefore, it will be interesting to explore the effect of 3s dopants (e.g., Al) on the CDW and SC in $CuIr_2Te_4$.

In this work, we prepared polycrystalline $CuIr_{2-x}Al_xTe_4$ ($0 \leqslant x \leqslant 0.2$) compounds successfully by a solid-state reaction method. Our results demonstrate that the CDW order can be completely suppressed within a fine-tuned Al-doped content as a result of the improvement of T_c. T_c initially increases with the rise of doping amount until $x = 0.075$ and reaches the highest value of 2.75 K, eventually forming a dome-phase like electronic phase diagram. The acquisition of the $CuIr_{2-x}Al_xTe_4$ ($0 \leqslant x \leqslant 0.2$) system also provides some enlightenment for the search of new superconductors.

2. Experimental methods

Synthesis Polycrystalline specimens of $CuIr_{2-x}Al_xTe_4$ ($0 \leqslant x \leqslant 0.2$) were prepared through the classical solid-state phase reaction. First, the Cu (99%, Alfa Aesar), Ir (99.9%, Macklin), and Al (99.95%, Aladdin) powder, and Te lump (99.999%, Alfa Aesar) with an element ratio of Cu : Ir : Al : Te = $1 : 2-x : x : 4.05$ were sealed in quartz tubes, then they were put in a muffle furnace with the ramping rate of 1 °C/min to 850 °C and the furnace temperature was maintained for 5 days. The resulting samples were annealed at 850 °C for 4 days with a heating rate of 1 °C/min.

Instruments Powder x-ray diffraction (PXRD) MiniFlex, Rigaku with Cu $K_{\alpha 1}$ radiation was used to examine the crystal structure and phase purity of the $CuIr_{2-x}Al_xTe_4$ ($0 \leqslant x \leqslant 0.2$) compounds. FULLPROF software suite was used to determine the cell parameters based on Thompson-Cox-Hastings pseudo-Voigt peak shapes model. Measurements of the temperature-dependence of electrical resistivity, specific heat, and magnetic susceptibilities ($M(T,H)$) were performed by a DynaCool Quantum Design physical property measurement system (PPMS, Quantum Design, Inc.).

3. Results and discussion

The PXRD patterns of the $CuIr_{2-x}Al_xTe_4$ compounds are presented in Fig. 1(a). PXRD analysis shows that Al concentration is limited up to 0.2 since Al_2Te_3 impurity is found with further increasing Al content. As Al doping content increases, the (001) peak moves to the right, which can be verified by the decrease of lattice constants a and c with increasing x (Fig. 1(c)), reflecting the compression of the $CuIr_2Te_4$ unit cell. As illustrated in Fig. 1(c) clearly, both lattice constants (a and c) and c/a singly reduce with increasing Al concentration. It is found that a and c reduce from 3.9397(5) Å and 5.3965 (3) Å for the pristine sample to 3.9264(1) Å and 5.3757(2) Å ($x = 0.2$) in $CuIr_{2-x}Al_xTe_4$, respectively. The detailed refinement of the selected sample $CuIr_{1.925}Al_{0.075}Te_4$ is displayed in Fig. 2(a).

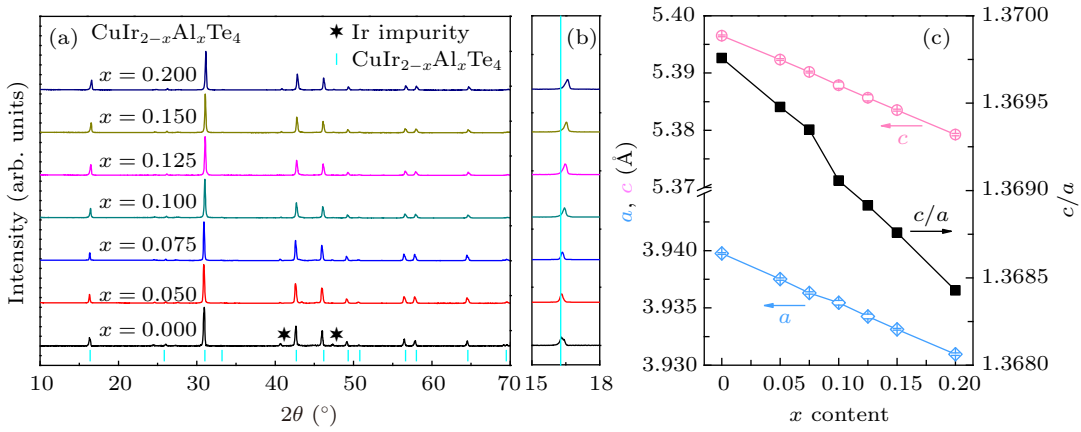


Fig. 1. (a) and (b) PXRD patterns of the $CuIr_{2-x}Al_xTe_4$ ($0 \leqslant x \leqslant 0.2$) compounds. (c) The evolution of lattice constants for $CuIr_{2-x}Al_xTe_4$ ($0 \leqslant x \leqslant 0.2$).

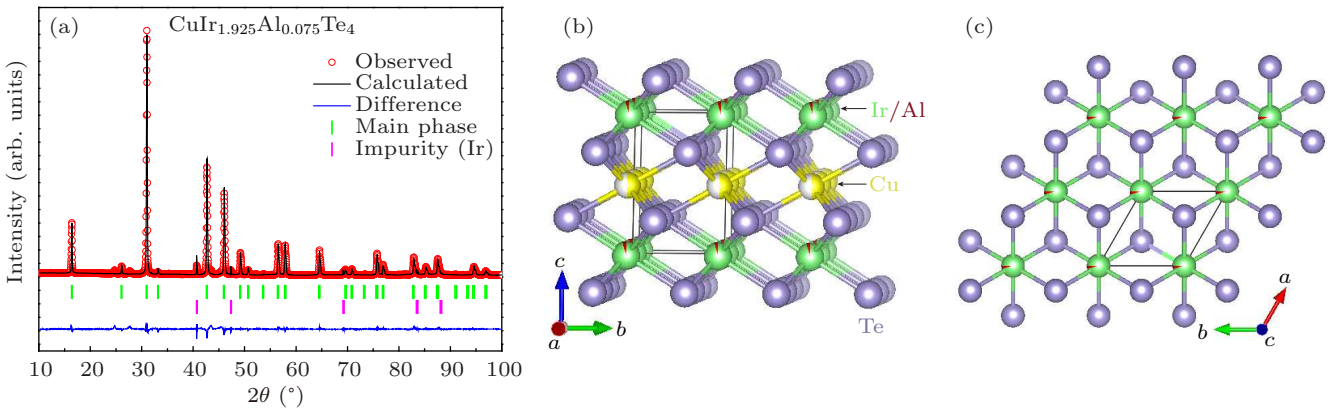


Fig. 2. (a) Refinements of $CuIr_{1.925}Al_{0.075}Te_4$ polycrystalline sample. (b) and (c) The crystal structure of $CuIr_{2-x}Al_xTe_4$ in different direction views.

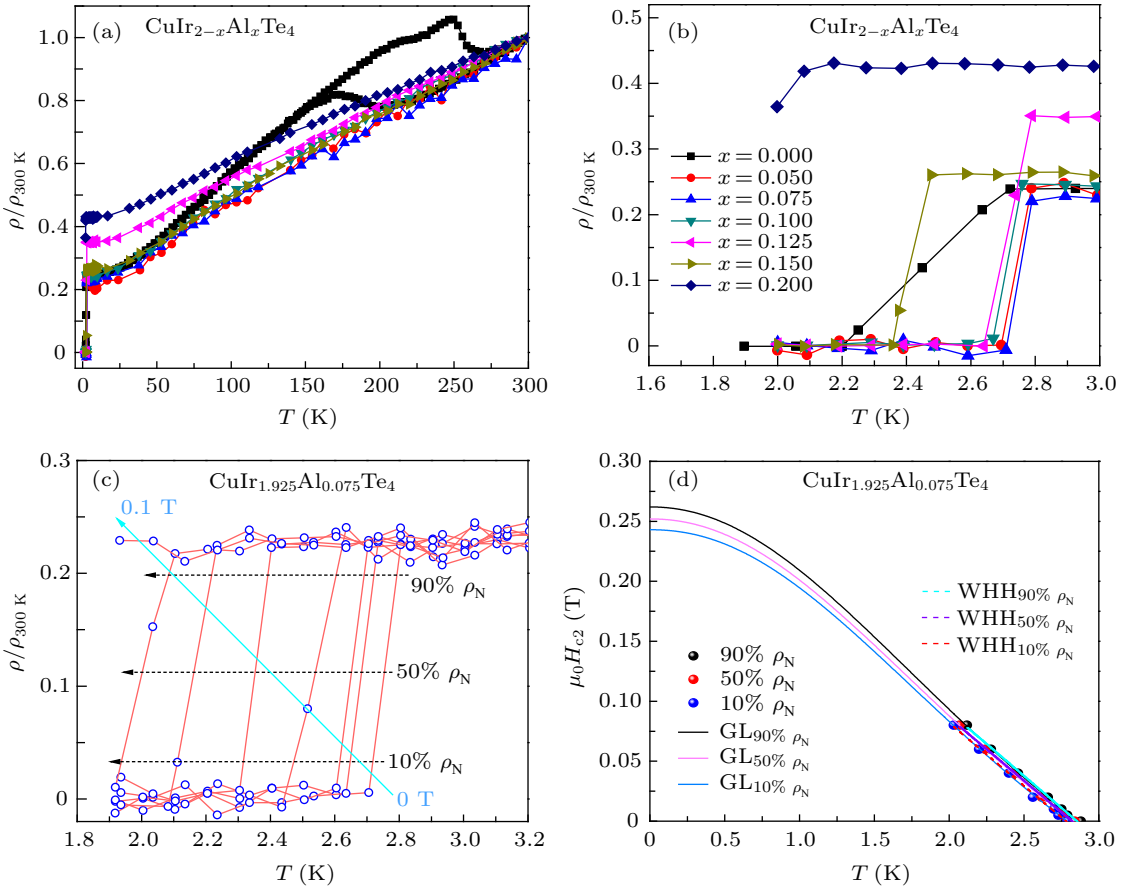


Fig. 3. (a) Temperature-dependence of resistivity for the polycrystalline $CuIr_{2-x}Al_xTe_4$ ($0 \leqslant x \leqslant 0.2$) compounds. (b) The superconducting transition at 1.6–3.0 K for the polycrystalline $CuIr_{2-x}Al_xTe_4$ ($0 \leqslant x \leqslant 0.2$) compounds. (c) Temperature dependences of resistivity for the polycrystalline $CuIr_{1.925}Al_{0.075}Te_4$ sample under various applied magnetic fields. (d) Temperature dependence of H_{c2} for the polycrystalline $CuIr_{1.925}Al_{0.075}Te_4$ sample.

Most of the diffraction peaks have been indexed in terms of trigonal symmetry with a space group P-3m1 (No. 164) and some small peaks indexed for tiny unreacted Ir are also detected. The illustration shows that the disordered trigonal structure, in which the Cu is inserted between two-dimensional (2D) $IrTe_2$ layers, Ir partial substituting by Al simultaneously (see Figs. 2(b) and 2(c)).

The temperature-dependent normalized resistivity ($\rho/\rho_{300\ \mathrm{K}}$) of the $CuIr_{2-x}Al_xTe_4$ ($0 \leqslant x \leqslant 0.2$) compounds is exhibited in Fig. 3(a). Besides, our previous finding indicates that there is no structure transition for the pristine sample. Thus, we propose that the normalized resistivity with cooling and heating exhibits a distinct hysteresis associated with the formation of CDW-like transition for the pristine $CuIr_2Te_4$ sample. It is worth mentioning that no signature of the abnormal hump can be observed above T_c in $\rho/\rho_{300\ \mathrm{K}}$ of the Al doping samples $CuIr_{2-x}Al_xTe_4$ ($0 < x \leqslant 0.2$), indicating the CDW-like transition can be suppressed with subtle Al substitution for Ir, companying with the increment of T_c. The resistivity data for Al-doped samples show a metallic behavior.

We can observe sharp drops of $\rho(T)$ for the $CuIr_{2-x}Al_xTe_4$ ($0 \leqslant x \leqslant 0.15$) below 3.0 K (see Fig. 3(b)), which represent the outset of the superconducting state. The transition width of the Al-doped compounds is much narrower than that of the pristine $CuIr_2Te_4$. The T_c and residual resistivity ratio (RRR $= R(300\ \mathrm{K})/R(3\ \mathrm{K})$) of the $CuIr_{2-x}Al_xTe_4$ ($0 \leqslant x \leqslant 0.2$) samples are summarized in Table 1. As the Al content increases, both T_c and RRR increase to the highest value at $x = 0.075$, then decrease for further Al doping. For $0.075 \leqslant x \leqslant 0.5$, the RRR sharply decreases form 4.44 for $x = 0.075$ to 2.342 for $x = 2.34$. This phenomenon indicates that high Al content induces significant disorder in the polycrystalline $CuIr_{2-x}Al_xTe_4$ series.

Table 1. The T_c and RRR of $CuIr_{2-x}Al_xTe_4$ ($0 \leqslant x \leqslant 0.2$) compounds. The T_c is determined by using 50% normal state resistance criterion.

x	T_c (K)	RRR
0	2.50	4.149
0.05	2.74	4.367
0.075	2.75	4.444
0.1	2.72	4.115
0.125	2.71	2.865
0.15	2.41	3.846
0.2		2.342

To evaluate the superconducting properties of the $CuIr_{1.925}Al_{0.075}Te_4$ compound with the highest T_c in detail, we have measured the resistivity under various applied magnetic fields. T_c's shift to lower temperature with the increasing applied field (see in Fig. 3(c)). The upper critical field $\mu H_{c2}(0)$ is obtained from Werthamer–Helfand–Hohenberg (WWH) and Ginzburg–Landau (GL) models. The upper critical field $\mu H_{c2}(T)$ values of $CuIr_{1.925}Al_{0.075}Te_4$ at zero temperature can be extrapolated by GL formula using the data deriving from 10%, 50%, and 90% criteria of ρ_N (normal-state resistivity). The GL formula is shown as follows: $\mu_0 H_{c2} = \mu_0 H_{c2}(0)^* \frac{1-(T/T_c)^2}{1+(T/T_c)^2}$.[47] The $\mu H_{c2}(0)$ values of 0.235 T, 0.250 T, and 0.255 T for $CuIr_{1.925}Al_{0.075}Te_4$ can be determined using the data 10%, 50% and 90% criteria of ρ_N, respectively. Furthermore, we can acquire the $\mu H_{c2}(0)$ values of 0.180 T, 0.191 T, and 0.193 T for $CuIr_{1.925}Al_{0.075}Te_4$ corresponding to the data 10%, 50%, and 90% criteria of ρ_N, respectively, via using the WHH formula $\mu H_{c2} = -0.693 T_c\, dH_{c2}/dT_c$ for the dirty limit SC.[48] The slopes, dH_{c2}/dT, are obtained from linear fitted $CuIr_{1.925}Al_{0.075}Te_4$ sample for data 10%, 50% and 90% criteria of ρ_N. Additionally, we fit the Pauli limiting field ($\mu H^P(T)$) by the formula $\mu H^P(T) = 1.86 T_c$, which is shown in Table 2. Then, the Ginzburg–Landau coherence length $\xi_{GL}(0)$ can be derived from the equation $\phi_0 \mu_0 H_{c2}(T) = \phi_0/(2\pi\xi_{GL}^2)$, where ϕ_0 represents the flux quantum. For example, $\xi_{GL}(0)$ of $CuIr_{1.925}Al_{0.075}Te_4$ is calculated to be 40.4 nm via using 50% criteria of ρ_N data based on WHH model. Table 2 summarizes all the relative experimentally measured and estimated parameters.

Table 2. Comparison of physical properties of $CuIr_2Te_4$-based superconductors.

Compound	$CuIr_{1.925}Al_{0.075}Te_4$	$CuIr_{1.925}Ti_{0.075}Te_4$ [33]	$CuIr_{1.95}Ru_{0.05}Te_4$ [32]	$CuIr_2Te_4$ [31]
T_c (K)	2.75	2.84	2.79	2.50
γ (mJ·mol^{-1}·K^{-2})	12.12	14.13	12.26	12.05
β (mJ·mol^{-1}·K^{-4})	2.20	2.72	1.87	1.97
Θ_D (K)	183.5(1)	170.9(1)	193.6(2)	190.3(1)
$\Delta C/\gamma T_c$	1.53	1.34	1.51	1.50
λ_{ep}	0.66	0.64	0.65	0.63
$N(E_F)$ (states/(eV·f.u))	3.13	3.67	3.15	3.10
μH_{c2} (T) (50% ρ_N WHH theory)	0.191	0.212	0.247	0.12
μH^P (T)	5.12	5.28	5.24	4.65
μH_{c1} (T)	0.060	0.095	0.098	0.028
$\xi_{GL}(0)$ (nm) (50% ρ_N WHH theory)	40.4	39.3	36.3	52.8

The superconducting transition has also been confirmed by the magnetic susceptibility data (Fig. 4(a)) with strong diamagnetic signals under zero-field-cooling (ZFC) mode. The superconducting volume fraction of the $CuIr_{2-x}Al_xTe_4$ ($0 \leqslant x \leqslant 0.15$) compounds can be calculated around 95%, which manifests high purity of the polycrystalline $CuIr_{2-x}Al_xTe_4$ samples. Next, we examine the lower critical fields (μH_{c1}) by the field-dependent magnetic susceptibility $M(H)$ measurements in a temperature range of 2–2.6 K. Figure 4(b) presents the magnetization (M–H) curves at different temperatures below T_c of the representative $CuIr_{1.925}Al_{0.075}Te_4$. As shown by the purple line in Fig. 4(b), the $M(H)$ isotherms show a linear relationship with the magnetic field (H) at low magnetic fields, indicating that it is a type-II superconductor. We can extract the demagnetization factor (N) following the expression $N = 4\pi\chi_V + 1$, where $\chi_V = dM/dH$ represents the linearly fitted slope. The calculated N for $CuIr_{1.925}Al_{0.075}Te_4$ is about 0.53. We can use the expression $M_{fit} = m + nH$ to fit the experimental data at low magnetic fields, where m represents the intercept and n stands for the slope of linear fitting from the low magnetic field $M(H)$ data. The inset of Fig. 4(c) displays the (M–M_{fit}) data vs. H. Then, we can fit the $\mu H_{c1}(T)$ by

the expression $\mu_0 H_{c1}(T) = \mu_0 H^*_{c1}(T)/(1-N)$, where $\mu_0 H^*_{c1}$ is the intersection point between the M–M_{fit} vs. H curves and the field (purple line in the inset of Fig. 4(c)), which deviates by ~1% above the fitted data (M_{fit}) as customary. The temperature dependence of $\mu_0 H_{c1}(T)$ for $CuIr_{1.925}Al_{0.075}Te_4$ is displayed in the main panel of Fig. 4(c). Consequently, we can further acquire the $\mu_0 H_{c1}(T)$ using the equation $\mu_0 H_{c1}(T) = \mu_0 H_{c1}(0)(1-(T/T_c)^2)$. The estimated $\mu_0 H_{c1}(0)$ at zero temperature of $CuIr_{1.925}Al_{0.075}Te_4$ sample is 0.060 T, which is larger than that of the undoped parent sample (see in Table 2).

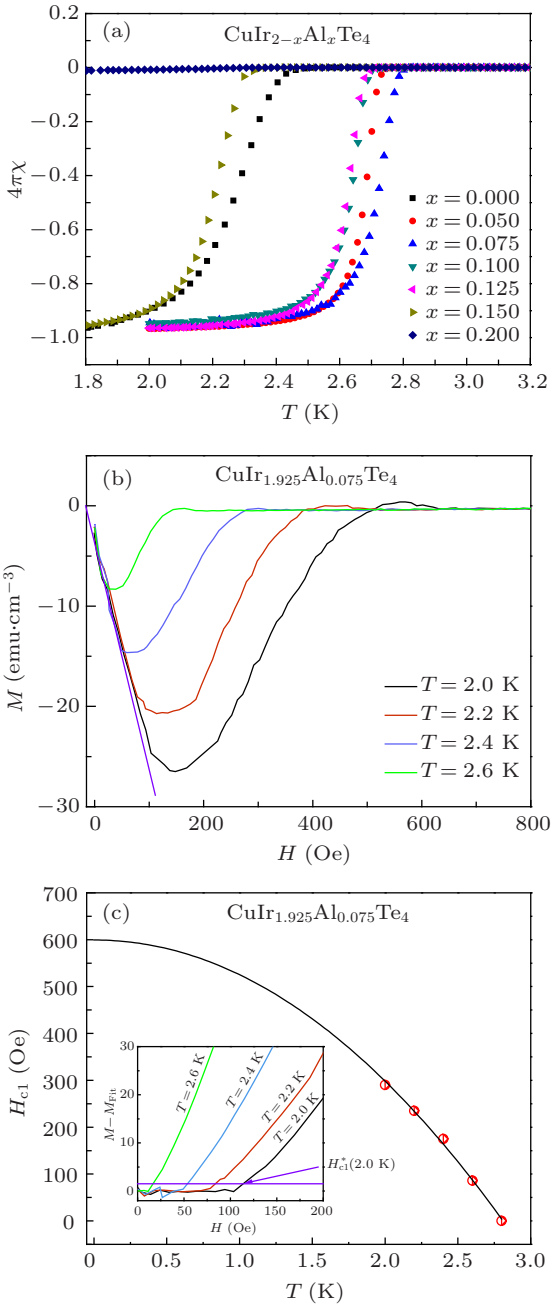


Fig. 4. (a) Magnetic susceptibility for $CuIr_{2-x}Al_xTe_4$ ($0 \leqslant x \leqslant 0.2$) compounds under 30 Oe magnetic field with zero-field-cooling (ZFC) mode. (b) The magnetization $M(H)$ in a temperature range of 2–2.6 K for $CuIr_{1.925}Al_{0.075}Te_4$. (c) Temperature dependence of H_{c1}. Inset: Difference between M and M_{Fit} in a temperature range of 2–2.6 K for $CuIr_{1.925}Al_{0.075}Te_4$.

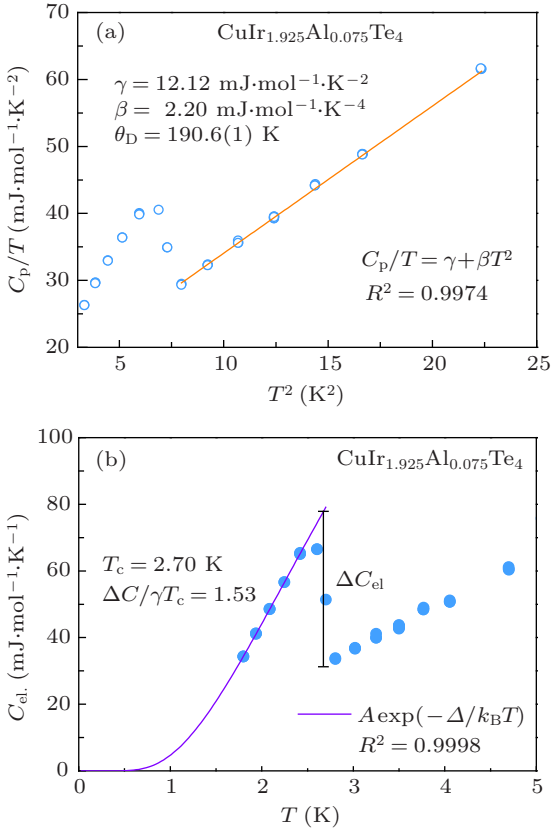


Fig. 5. (a) The specific heat data plotted as a function of T^2 for $CuIr_{1.925}Al_{0.075}Te_4$. (b) The electronic part of the specific heat in $CuIr_{1.925}Al_{0.075}Te_4$.

To further convince that SC is an essential feature of the highest T_c compound $CuIr_{1.925}Al_{0.075}Te_4$, we also perform the temperature-dependent specific heat measurement. Figure 5 illustrates the detailed characterization of the superconducting transition in the highest T_c composition $CuIr_{1.925}Al_{0.075}Te_4$ through specific heat measurements under the absence of magnetic field. The data C_p/T vs. T^2 can be fitted by the equation $C_p = \gamma T + \beta T^3$ above the T_c to acquire the values of β and γ being 2.20 mJ·mol^{-1}·K^{-4} and 12.12 mJ·mol^{-1}·K^{-2} for $CuIr_{1.925}Al_{0.075}Te_4$, respectively, where γT represents the sum of electron contributions ($C_{el.}$) to the specific heat and βT^3 is the sum of phonon contributions ($C_{ph.}$). Figure 5(b) shows the sum of electron contribution to the specific heat at the temperature near the T_c under 0 T, where $C_{el.}$ is easily derived from deducting the phonon part, $C_{el.} = C_p - \beta T^3$. Apparently, a sharp specific heat jump occurs in our representative $CuIr_{1.925}Al_{0.075}Te_4$, characteristic of bulk SC. The T_c further can be determined to be 2.70 K using the common equal-area entropy construction method, which agrees well with those observed in magnetization and resistivity tests. Based on the T_c and γ values, we can determine $\Delta C_{el.}/(\gamma T_c) = 1.53$, which is slightly larger than the value of 1.43 forecasted by the BCS theory, revealing its superconducting nature. The Debye temperature obtained using the equation $\Theta_D = (12\pi^4 nR/(5\beta))^{1/3}$ is 183.5(1) K, where R represents the gas constant, n expresses the number of atoms per formula unit. The resultant electron–

phonon coupling constant λ_{ep} value further estimated by introducing the Θ_D number into the inverted McMillan equation[49]

$$\lambda_{ep} = \frac{1.04 + \mu^* \ln\left(\frac{\Theta_D}{1.45T_c}\right)}{(1-0.62\mu^*)\ln\left(\frac{\Theta_D}{1.45T_c}\right) - 1.04}$$

for $CuIr_{1.925}Al_{0.075}Te_4$ is 0.66. Following the formula $N(E_F) = \frac{3}{\pi^2 k_B^2 (1+\lambda_{ep})}\gamma$, the λ_{ep} and γ values can give the electron density of states (DOSs) around the Fermi level ($N(E_F)$). The obtained $N(E_F) = 3.13$ states/(eV·f.u.) for $CuIr_{1.925}Al_{0.075}Te_4$, is greater than that of pristine $CuIr_2Te_4$ (($N(E_F) = 3.1$ states/(eV·f.u)). The enhancement of T_c may be accompanied by the increment of the DOS states at the Fermi energy in $CuIr_{2-x}Al_xTe_4$ systems. As show in Fig. 5(b), the specific heat data can be basically fit with the equation $C_{el} = A\exp(-\Delta/(k_B T))$. Due to the limitation of experimental conditions, the specific heat measurement did not measure the lower temperature region. Nevertheless, the R^2 value of 0.9998 shows that the data and the calculated curve are reasonably consistent.

Finally, to further understand the effect of Al dopant on the CDW and SC of $CuIr_2Te_4$, the electronic phase diagrams plotted as T_c versus Al-content x have been established (see Fig. 6). All the T_c values were obtained from the resistivity and magnetization tests. From Fig. 6, we can find that the CDW order is immediately suppressed while T_c increases with increasing Al content up to $x = 0.075$ and rises towards the highest value 2.75 K at $x = 0.075$. From this, we find that despite subtle Al is substituted for Ir, it has a strong impact on the SC and CDW. Besides, in contrast to our previously reported Ru/Ti-doped $CuIr_2Te_4$ system, the similarity is the destabilization of CDW upon small amount doping concentration no matter Ru, Ti, or Al as dopants and formation of dome-shape like superconducting phase diagrams.[32,33] Despite overall similarities, there are significant differences between the $CuIr_{2-x}Ru_xTe_4$, $CuIr_{2-x}Ti_xTe_4$, and $CuIr_{2-x}Al_xTe_4$ systems. Substitution of Ir by Ru or Ti in $CuIr_2Te_4$ corresponds to a "hole" (p-type) doping of the $IrTe_2$ layers, while partial doping Al into Ir site in $CuIr_2Te_4$ is an electron (n-type) doping. As for the high-T_c cuprate superconductors, where the competition between antiferromagnetism and SC develops as a function of chemical doping, the evolving balance between competing electronic orders in CDW/SC systems is one of their most fundamentally tempting properties. In our case, the bands in the neighborhood of the Fermi energy E_F of the pristine sample $CuIr_2Te_4$ mostly come from Ir d and Te p orbitals and locate at a flat plateau, in which Al doping acts as a chemical pressure, closing the gap on the Fermi surface that usually leads to rapid suppression of CDW. On the other hand, the increase of band filling of the Fermi surface under chemical pressure could be the mechanism of the promotion of SC. But further study and evidence need to be collected to find out the competition between CDW and SC.

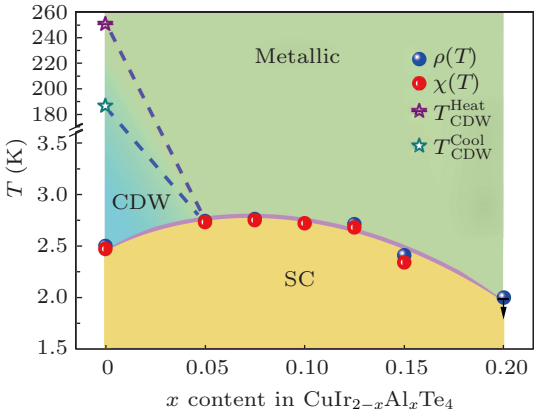


Fig. 6. The electronic phase diagram of polycrystalline $CuIr_{2-x}Al_xTe_4$ ($0 \leqslant x \leqslant 0.2$) series.

4. Conclusion and perspectives

In conclusion, we have successfully synthesized a series of polycrystalline $CuIr_{2-x}Al_xTe_4$ ($0 \leqslant x \leqslant 0.2$) samples via a solid-state method and systemically studied the effect of Al doping on the structure and electronic properties of $CuIr_2Te_4$. The $\Delta C_{el.}/(\gamma T_c) = 1.53$ for the highest T_c sample $CuIr_{1.925}Al_{0.075}Te_4$ is slightly larger than 1.43 (BCS value), proving its bulk superconducting nature. We recognize that the CDW order is suppressed immediately while T_c increases as Al doping amount x rises and achieves a maximum $T_c =$ 2.75 K with Al doping content of 0.075. Our systematic study of $CuIr_{2-x}Al_xTe_4$ ($0 \leqslant x \leqslant 0.2$) not only extends the family of the TMD superconductors but also provides a platform for further research on the relationship between the CDW and SC.

Acknowledgments

H. X. Luo acknowledges the financial support by the National Natural Science Foundation of China (Grant No. 11922415), Guangdong Basic and Applied Basic Research Foundation, China (Grants No. 2019A1515011718), and the Pearl River Scholarship Program of Guangdong Province Universities and Colleges (Grants No. 20191001). Y. Zeng and D. X. Yao are supported by the National Natural Science Foundation of China (Grants No. 11974432) and the National Key R&D Program of China (Grant Nos. 2018YFA0306001 and 2017YFA0206203). D. Yan acknowledges the financial support by the National Key Laboratory Development Fund (No. 20190030). Y. H. Wang would like to acknowledge partial support by the National Key R&D Program of China (Grant No. 2017YFA0303000), National Natural Science Foundation of China (Grant No. 11827805), and Shanghai Municipal Science and Technology Major Project, China (Grant No. 2019SHZDZX01). M. Wang was

supported by the National Natural Science Foundation of China (Grant Nos. 11904414 and 12174454) and the National Key R&D Program of China (Grant No. 2019YFA0705702).

References

[1] Doan P, Gooch M, Tang Z J, Lorenz B, Möller A, Tapp J, Chu P C W and Guloy A M 2012 *J. Am. Chem. Soc.* **134** 16520

[2] Mososan E, Zandbergen H W, Dennis B S, Bos J W G, Onose Y, Klilmczuk T, Ramirez A P, Ong N P and Cava R J 2006 *Nat. Phys.* **2** 544

[3] Shen B, Du F, Li R, Thamizhavel A, Smidman M, Nie Z Y, Luo S S, Le T, Hossain Z and Yuan H Q 2020 *Phys. Rev. B* **101** 144501

[4] Fang L, Wang Y, Zou P Y, Tang L, Xu Z, Chen H, Dong C, Shan L and Wen H H 2005 *Phys. Rev. B* **72** 014534

[5] Zhao Z X, Chen L Q, Yang Q S, Huang Y Z, Chen G H, Tang R M, Liu G R, Cui C G, Chen L, Wang L Z, Guo S Q, Li S L and Bi J Q 1987 *Chin. Sci. Bull.* **32** 412

[6] Wu M K, Ashburn J R, Torng C J, Hor P H, Meng R L, Guo L, Huang Z J, Wang Y Q and Chu C W 1987 *Phys. Rev. Lett.* **58** 908

[7] Sasmal K, Lv B, Lorenz B, Guloy A M, Guloy F, Xue Y Y and Chu C W 2008 *Phys. Rev. Lett.* **101** 107007

[8] Chuang T M, Allan M P, Lee J, Xie Y, Ni N, Bud'ko S L, Boebinger G S, Canfield P C and Davis J C 2010 *Science* **327** 181

[9] Ren Z A, Lu W, Yang J, Yi W, Shen X L, Li Z C, Che G C, Dong X L, Sun L L and Zhao Z X 2008 *Chin. Phys. Lett.* **25** 2215

[10] Mao Y Y, Li J, Huang Y L, Yuan J, Li Z A, Chai K, Ma M W, Ni S L, Tian J P, Liu S B, Zhou H X, Zhou F, Li J Q, Zhang G M, Jin K, Dong X L and Zhao Z X 2018 *Chin. Phys. Lett.* **35** 057402

[11] Yang J, Zhou R, Wei L L, Yang H X, Li J Q, Zhao Z X and Zheng G Q 2015 *Chin. Phys. Lett.* **32** 107401

[12] Dong X L, Jin K, Yuan J, Zhou F, Zhang G M and Zhan Z X 2018 *Acta Phys. Sin.* **67** 207410 (in Chinese)

[13] Hong X C, Wang A F, Zhang Z, Pan J, He L P, Luo X G, Chen X H and Li S Y 2015 *Chin. Phys. Lett.* **32** 127403

[14] Joe Y I, Chen X M, Ghaemi P, Finkelstein K D, de la Pena G A, Gan Y, Lee J C T, Yuan S, Geck J, MacDougall G J, Chiang T C, Cooper S L, Fradkin E and Abbamonte P 2014 *Nat. Phys.* **10** 421

[15] Yan D, Lin Y S, Wang G H, Zhu Z, Wang S, Shi L, He Y, Li M R, Zheng H, Ma J, Jia J F, Wang Y H and Luo H X 2019 *Supercond. Sci. Technol.* **32** 085008

[16] Luo H X, Xie W W, Tao J, Inoue H, Gyenis A, Krizan J W, Yazdani A, Zhu Y M and Cava R J 2015 *Proc. Natl. Acad. Sci. USA* **112** E1174

[17] Liu Y, Bao J J, Xu C Q, Jiao W H, Zhang H, Xu C L, Zhu Z, Yang H Y, Zhou Y H, Ren Z, Biswas P K, Ghosh S K, Yang Z, Ke X, Cao G H and Xu X F 2021 *Phys. Rev. B* **104** 104418

[18] Xing Y, Yang P, Ge J, Yan J J, Luo J W, Ji H R, Yang Z Y, Li Y J, Wang Z J, Liu Y Z, Yang F, Qiu P, Xi C Y, Tian M L, Liu Y, Lin X and Wang J 2021 *Nano Lett.* **21** 7486

[19] Xing Y, Zhao K, Shan P J, Zheng F P, Zhang Y W, Fu H L, Liu Y, Tian M L, Xi C Y, Liu H W, Feng J, Lin X, Ji S H, Chen X, Xue Q K and Wang J 2017 *Nano Lett.* **17** 6802

[20] Li X Q, Li Z L, Zhao J J and Wu X S 2020 *Chin. Phys. B* **29** 87402

[21] Simchi H 2020 *Chin. Phys. B* **29** 27401

[22] Qi Y P, Naumov P G, Ali M N, *et al*. 2016 *Nat. Commun.* **7** 11038

[23] Chen P, Pa W W, Chan Y H, Takayama A, Xu C Z, Karn A, Hasegawa S, Chou M Y, Mo S K, Fedorov A V and Chiang T C 2017 *Nat. Commun.* **8** 516

[24] Zhou M H, Li X C and Dong C 2018 *Supercond. Sci. Technol.* **31** 065001

[25] Luo H X, Xie W W, Tao J, Pletikosic I, Valla T, Sahasrabudhe G S, Osterhoudt G, Sutton E, Burch K S, Seibel E M, Krizan J W, Zhu Y M and Cava R J 2016 *Chem. Mater.* **28** 1927

[26] Sipos B, Kusmartseva A F, Akrap A, Berger H, Forro L and Tutis E 2008 *Nat. Mater.* **7** 960

[27] Ye J T, Zhang Y J, Akashi R, Bahramy M S, Arita R and Iwase Y 2012 *Science* **338** 1193

[28] Kusmartseva A F, Sipos B, Berger H, Forró L and Tutiš E 2009 *Phys. Rev. Lett.* **103** 236401

[29] Fang L, Wang Y, Zou P Y, Tang L, Xu Z, Chen H, Dong C, Shan L and Wen H H 2005 *Phys. Rev. B* **72** 014534

[30] Hu W Z, Li G, Yan J, Wen H H, Wu G, Chen X H and Wang N L 2007 *Phys. Rev. B* **76** 045103

[31] Yan D, Wang S, Lin Y S, Wang G H, Zeng Y J, Boubeche M, He Y, Ma J, Wang Y H, Yao D X Luo H X 2020 *J. Phys.: Condens. Matter* **32** 025702

[32] Kiswandhi A, Brooks J S, Cao H B, Yan J Q, Mandrus D, Jiang Z and Zhou H D 2013 *Phys. Rev. B* **87** 121107(R)

[33] Zeng J W, Liu E F, Fu Y J, *et al.* 2018 *Nano Lett.* **18** 1410

[34] Wagner K E, Morosan E, Hor Y S, Tao J, Zhu Y M, Sanders T, McQueen T M, Zandbergen H W, Williams A J, West D V and Cava R J 2008 *Phys. Rev. B* **78** 104520

[35] Pan X C, Chen X L, Liu H M, Feng Y Q, Wei Z X, Zhou Y H, Chi Z H, Pi L, Yen F, Song F Q, Wan X G, Yang Z R, Wang B G and Zhang Y H 2015 *Nat. Commun.* **6** 7805

[36] Yu Y J, Yang F Y, Lu X F, Yan Y J, Cho Y H, Ma L G, Niu X H, Kim S, Son Y W, Feng D L, Li S Y, Cheong S W, Chen X H and Zhang Y B 2015 *Nat. Nanotech.* **10** 270

[37] Luo J W, Li Y A, Zhang J W, Ji H R, Wang H, Shan J Y, Zhang G X, Cai C, Liu J, Wang Y, Zhang Y and Wang J 2020 *Phys. Rev. B* **102** 064502

[38] Li Y A, Gu Q Q, Chen C, Zhang J, Liu Q, Hu X Y, Liu J, Liu Y, Ling L S, Tian M L, Wang Y, Samarth N, Li S Y, Zhang T, Feng J and Wang J 2018 *Proc. Natl. Acad. Sci. USA* **115** 9503

[39] Yan D, Zeng Y J, Wang G H, Liu Y Y, Yin J J, Chang T R, Liu H, Wang M, Ma J, Jia S, Yao D X and Luo H X 2019 arXiv: 1908.05438

[40] Yan D, Zeng L Y, Lin Y S, Yin J J, He Y, Zhang X, Huang M L, Shen B, Wang M, Wang Y H, Yao D X and Luo H X 2019 *Phys. Rev. B* **100** 174504

[41] Zeng L Y, Yan D, He Y Y, Boubeche M, Huang Y H, Wang X P and Luo H X 2021 *J. Alloys Compd.* **885** 160981

[42] Boubeche M, Yu J, Li C S, Wang H C, Zeng L Y, He Y Y, Wang X P, Su W Z, Wang M, Yao D X and Luo H X 2021 *Chin. Phys. Lett.* **38** 037401

[43] Boubeche M, Wang N N, Sun J P, Yang P T, Zeng L Y, Li Q Z, He Y Y, Luo S J, Cheng J G, Peng Y Y and Luo H X 2021 *Supercond. Sci. Tech.* **34** 115003

[44] Antal V, Kanuchova M, Šefčiková, M, Kovac J, Diko P, Eisterer M, Hörhager N, Zehetmayer M, Weber H W and Chaud X 2009 *Supercond. Sci. Technol.* **22** 105001

[45] Scavini B, Malavasi L and Mollica L 2004 *Solid. State. Sci.* **6** 1187

[46] Ansari I 2017 *J. Mod. Mater.* **3** 33

[47] Ginzburg V L 1955 *Nuovo. Cim.* **2** 1234

[48] McMillan W L 1968 *Phys. Rev. B* **167** 331

[49] Bardeen J, Cooper L N and Schrieffer J R 1957 *Phys. Rev.* **108** 1175